PCCP

Simulation of powder diffraction patterns of modified ordered mesoporous materials

Jürgen Sauer,† Frank Marlow and Ferdi Schüth

MPI für Kohlenforschung, Kaiser-Wilhelm-Platz 1, 45470 Mülheim, Germany.
E-mail: schueth@mpi-muelheim.mpg.de; Tel: +49-208-306 2373; Fax: +49-208-306 2995

Received 14th September 2001, Accepted 26th October 2001
First published as an Advance Article on the web

Powder diffraction patterns of ordered mesoporous materials are simulated with a newly developed program, which allows investigation of the influence of any desired matter distribution in the unit cell on the diffraction pattern. The simulation process can be subdivided into two major steps. First, a unit cell is generated from SiO_2 and, optionally, other building units. A weighted random placement of atoms is used to simulate the distribution of different atoms in different parts of the unit cell. This is done by a Fermi-type function, by which the probability of finding an atom on a site depends on the distance of a point from the center of a pore, leading to a smooth, continuous transition from wall to pore. Secondly, structure factors and then intensities of reflections are calculated, using the Lorentz correction and a geometric correction for powder data. The use of this program is demonstrated by the simulation of diffraction patterns, mainly for unmodified and modified SBA-15 as well as for MCM-41. Good agreement of simulated and experimental data is observed.

Introduction

Ordered mesoporous materials discovered by Kresge *et al.*[1] and Yanagisawa *et al.*[2] have generated tremendous interest over the last ten years. The state of the art is documented in several recent review articles,[3–6] and now various different structures and framework compositions can be synthesized. One possible application of ordered mesoporous silica is as a host material for various guest species. These can be anchored to the walls, spread in a monolayer on the walls, be present in the pore system as particles, or completely fill the void space of the structure. There are examples for all of these possible distributions of the guest species in the pore system. We recently described the loading of ordered mesoporous silica of the SBA-15-type with rare earth oxides which led to a spreading of the rare earth oxide on the channel surface of the host silica.[7,8] In connection with this work, unexpected variations in the relative intensities of the low angle reflections in the X-ray diffraction patterns were observed with increasing loading, *i.e.* disappearance of reflections at relatively low loading and reappearance at higher loading levels. In order to understand this behavior, a structural model for loaded ordered mesoporous materials was developed which is able to explain the observed changes in diffraction intensities and which is sufficiently general to allow also the simulation of the diffraction patterns for many other cases.

Before the model and the results for the diffraction patterns of oxide loaded SBA-15 are described in more detail, the different approaches taken so far to simulate XRD patterns for MCM-41 type materials will be discussed. Although very interesting results have been obtained, none of the procedures seem to fully cover the requirements for our calculations.

In one of the first publications by the Mobil group[9] an attempt was made to understand the diffraction behavior using the cylindrical shell model of Oster and Riley[10] or a zeolite-like model based on the 81(n) series.[11] Both models reproduced the experimental data quite satisfactorily. Since the Oster–Riley model is based on a continuous distribution of scattering matter, the Smith–Dytrych model on discrete silicate tetrahedra, Beck *et al.* concluded that X-ray structural modeling was only of limited use, for determination of the internal, short-range structure of the pore walls. Although this is true to some extent, later publications have shown that X-ray diffraction modeling can give insight into the distribution of matter on a larger scale. Also in one of the earlier publications it was mentioned that the observed diffraction patterns could be modeled better by a hexagonal pore structure than by a cylindrical one,[12] which was confirmed for MCM-41 experimentally[13] as well as in a more comprehensive later modeling study.[14] X-ray modeling has also been used to estimate the wall thickness of ordered mesoporous materials. Feuston and Higgins[15] have shown that the intensity ratios of the different reflections depend on the ratio between the wall thickness and the unit cell size. Their model structure for MCM-41 was rather more realistic in that it was obtained by a molecular dynamics simulation which allowed them to obtain at least theoretical information on the wall structure. A similar simulation was later used by Kleestorfer *et al.*[16] This simulation converged to a wall structure resembling amorphous silica, although the starting point was the quartz structure with holes of the dimension of the MCM-41 pores. Evidence for some local structuring in the walls was however obtained by analyzing the radial distribution function obtained from wide angle X-ray diffraction, in which good fits using structural subunits from the α-cristobalite structure could be achieved.[17] No X-ray diffraction modeling was given in that publication, but a simple model based on distorted crystalline silica had been used before to simulate diffraction patterns and assess the influence of irregularity and domain size on the experimental patterns.[18]

Most relevant for the purpose of the present study, however, are the publications by Hammond *et al.*[19] and Tun and Mason.[20] In these two papers, the problem of the filling of the channels with matter has been specifically addressed.

† Present address: Institut für Physikalische Chemie, LMU München, Germany.

Hammond *et al.* used a lattice model with hexagonal channels and different scattering form factors for the wall and the matter in the channel. They discussed the situation where the whole interior of the channel is filled. By varying the relative scattering form factors for the matter in the pores (in the study surfactant was assumed to be present), the effect of different degrees of pore filling or differently scattering matter on the reflection intensities could be modeled. Tun and Mason concentrated primarily on the effect of disorder on the diffraction pattern (using a model consisting of hexagonally packed cylinders), but in the last section also addressed the question of pore filling with different material. The authors distinguish two cases, first complete filling, which will just result in a difference in the contrast factor between wall and pores, and second, coating of the pores. This situation is more difficult, and only the case of a contrast matched coating is discussed in more detail. Two models also relevant for the present study were developed by Edler *et al.*[21] and Imperor-Clerc *et al.*[22] The first authors used a two-shell model with a dense wall center and a second layer of lower density, to fit the XRD patterns of very high quality MCM-41. A two-shell model was also used to gain insight into the partially microporous nature of SBA-15. Different models for the two shells were assumed and expressed in analytical functions, *i.e.* the two-cylinder model discussed previously, also including a Debye–Waller factor to simulate "smearing out" of the electron densities of the two cylinders, a model with a high core density and a lower "corona" density at the surface of the channel wall and a model with linearly decreasing density of silica towards the wall center after a dense wall core. The corona models were most successful in fitting the experimental patterns.

However, there is a disadvantage in using analytical functions to describe matter distribution in the unit cell (although it allows more facile calculations of the diffraction patterns). More irregular distributions of atoms in the unit cell are increasingly difficult to describe analytically, and also subsequent transformations are more complex. Thus, in order to allow approximation of the more complex situation in loaded ordered mesoporous materials and to develop a simple, general model for the simulation of diffraction patterns, we decided to formulate a computer model to generate distributions of scattering matter in a unit cell which should allow (i) the simulation of various pore shapes (ii) smooth transitions from wall to channel instead of a step transition, and (iii) the simulation either of channels partly filled with particles or of coated walls.

Methods

In the following the principle on which the program to simulate the diffraction patterns is based will be introduced. The full program including the source code is available free of charge from the authors upon request.

The diffraction patterns are calculated in four major steps:

(i) Generation of a structural model: First, a two-dimensional unit cell is generated. Since only the hexagonal *P*6 member of the family of ordered mesoporous materials is considered here and these materials in general do not exhibit periodicity in the direction of the crystallographic *c*-axis, the third dimension need not be taken into account. However, in principle, three-dimensional structures can also be investigated using our approach. In order to create the possibility of a quasi-continuous distribution of matter, 10^5 points with random co-ordinates are selected in this cell. We were mainly interested in the simulation of the loading of SBA-15, which has more or less cylindrical channels but the other materials discussed in this paper, SBA-3 and titanium oxophosphate, can probably also be well approximated by cylindrical channels. Thus, we used a radius r for the description of matter distribution, with $r = 0$ in the center of the channel. Then a number of random points were generated and a site occupation factor (N) for SiO_2 was assigned to them. This was set to 1 for points clearly lying in the wall and zero for points clearly lying in the pores. It should be stressed here, that any other channel geometry could be created just by applying different rules for the assignment of site occupation factors in the unit cell. In order to be able to simulate other than discontinuous transitions from pore to wall, continuous functions have been used to allow for occupation factors between 0 and 1 in the transition region. Here we used a Fermi-type function

$$P_{\mathrm{Fermi}} = \frac{1}{1 + \exp((r_0 - r)/\lambda)} \qquad (1)$$

which allows us to model also the influence of rough or partially porous walls on the diffraction pattern. Fermi-type functions change their value from 0 to 1 with adjustable slope, as shown in Fig. 1. In eqn. (1), r_0 is the pore radius, which can be chosen, r is the distance of the respective point from the center of the pore, and λ is the "smoothing parameter". The higher this parameter, the smoother the edges (see also Fig. 1).

For simulation of loading with guest species, different situations can be modeled by different assignments of the site occupation factors for the guest species. For instance, a coating of the channel walls is simulated by assigning non-zero occupation factors to points lying in the pores between r_0 (at the wall) and r_1 where $r_0 - r_1$ corresponds to the thickness of the coating. Here again, the transitions between the different regions are smoothed by a Fermi-type function. Partial filling of the channels can be simulated by assigning an occupation factor, corresponding to the degree of filling, to all points lying in the channels, *i.e.* for a homogeneous 30% filling of the channels all occupation factors for points in the channel are set at 0.3. To a first approximation, this corresponds to cylindrical particles filling 30% of the void volume. If spherical particles filling the channels are to be simulated, occupation factors in the center of the channel have to be adjusted to higher values than near the walls according to $\sqrt{r_0^2 - r^2}$, since the 3-D sphere is projected onto the 2-D unit cell. Using this procedure, it is possible to simulate different average distributions of matter in the unit cell. Fig. 2 shows the distribution of atoms for a simulated unit cell with an approximately monolayer coating of yttria on the channels of the structure.

(ii) The next step is the calculation of a *mean* form-factor for SiO_2 and, optionally, other condensed matter present for a certain reflection. For example, the mean form factor for SiO_2 is calculated according to eqn. (2).

$$f_{\mathrm{SiO_2}} = \frac{f_{\mathrm{Si}} + 2f_{\mathrm{O}}}{3} \qquad (2)$$

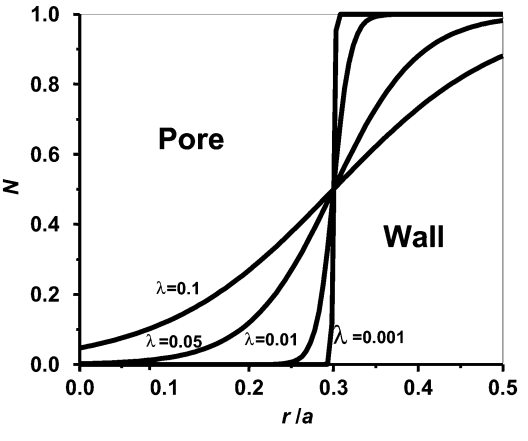

Fig. 1 Course of Fermi-type functions with different smoothing parameter λ.

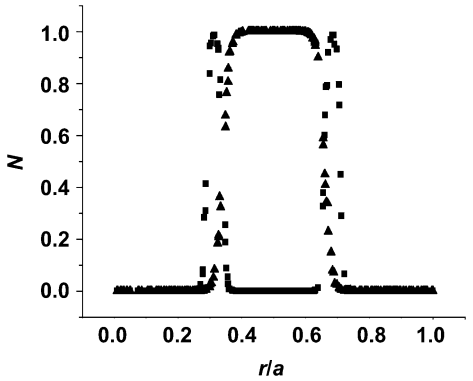

Fig. 2 Plot of site occupation factors N of Y_2O_3 (■) and SiO_2 (▲) for all points lying in a corridor of 0.1 nm thickness centered on the diagonal of the unit cell. ($a = 10$ nm, $\lambda = 0.005$ for all transitions, pore radius (without yttria layer) = 3.4 nm, thickness of Y_2O_3 layer = 0.6 nm).

Form factors for other oxides or other guest species can be obtained similarly. The form factors are calculated for different diffraction angles according to an algorithm adapted from ref. 23.

(iii) The third, major, step is the calculation of the structure factor. This is done by a summation, extending over all points in the unit cell, of the form factors weighted by the occupation factors multiplied by the phase factor. If more than one guest species is to be simulated, then the expression in brackets in eqn. (3) has to be expanded by another term for the additional guest species.

$$F_{hk} = \sum (f_{SiO_2}/N_{SiO_2} + f_{guest}N_{guest}) \cos(2\pi(xh + yk)) \qquad (3)$$

The summation is carried out over all sites generated by the program. The imaginary term of the phase factor is omitted, because the unit cell is inversion symmetric.

For simulations of the X-ray diffraction patterns and the following discussion, we have only considered the first four reflections, namely the (10), the (11), the (20), and the (21) reflection, since these are typically the ones which can be observed in a standard diffraction experiment on ordered mesoporous materials. The reflection intensities are calculated by multiplying the structure factor by itself and the multiplicity. (6 for all reflections except the (21) reflection which exhibits a multiplicity of 12).

(iv) In the last major step two angular dependent corrections for the reflection intensities are applied: the Lorentz correction and the geometric correction for powder diffraction patterns.[24]

This way of modeling contains some simplifying assumptions, which, however, do not substantially affect the results of the simulation in the important angle range. First, we used an average form factor for the silica and the guest species and performed a quasi-continuum modeling by using a high number of sites. This seems to be justified, since there is general agreement that the degree of long-range order within the walls is low. Moreover, the ordering in the wall would primarily affect the intensities at higher angles, not in the low-angle region we are interested in. Generally, omitting the third spatial dimension when calculating the diffraction pattern might also be considered a problem for two reasons. First, if there is periodicity in this direction, this would be removed from the simulated diffraction pattern. However, there is agreement, that for most of the materials there is no order in this direction and thus the two-dimensional quasi-continuum model can be used without loss of information. The second problem is related to the fact that for the silica walls there is a clear correlation between silicon and oxygen centers due to the typical bond geometry which is not taken into account here, since we used an averaged SiO_2 form factor. It could be recalculated to reflect correlation effects. However, this would not appreciably affect the results of this work in the low-angle region. The correlation between silicon and oxygen is known to contribute to intensity in the mid-angle range, centered at about 24° using copper radiation, such as for glasses and amorphous silica, a range we are not interested in for the purpose of this study.

Results of the simulation

Pure mesostructured and mesoporous silica

Fig. 3 shows the effect of changing wall thickness (since wall thickness is not uniform for cylindrical pores, wall thickness is taken as the thickness in the (10) direction) for a given unit cell size on the overall intensity of the (10) reflection. As expected, for a solid material of constant density ($r_0 = 0$) and for a wall thickness of 0 ($r_0 = 0.5$, corresponding to no continuous walls, but just patches of matter in the center of the unit cell), there is no or almost no (10) reflection observed. In between, the intensity passes through a maximum at a ratio between wall thickness and pore size of approximately 1 : 2. Most ordered mesoporous oxides have a ratio between wall thickness and pore size of between 0.5 and 0.25, so for such samples high intensity in the XRD for the (10) reflection would be expected.

However, absolute intensities can only be compared for different materials if it is ascertained that the same volume of matter is contributing to the scattering, which can in some cases be difficult to achieve experimentally. Information can actually be extracted more easily than from absolute intensities by the analysis of relative intensities of different reflections in one diffraction pattern. A high intensity in the low-angle range with rapid intensity decay for high angles would be indicative of thick walls, while lower intensity in the lower-angle range with a less pronounced fall-off with angle would indicate rather thinner walls. Strictly, since form factors and thus intensities change with angle, the relative intensities for materials of different unit cell size cannot be compared directly. However, for the different materials considered here, the unit cell sizes are almost identical and the changes in form factors in the relevant angle range are small. In addition the changes in form factors with angle are almost parallel for the different species involved. One should, nevertheless, keep in mind when using figures where the radii are normalized to the constant unit cell, that the calculations are exact only for the unit cell size for which they have been performed, and that for a

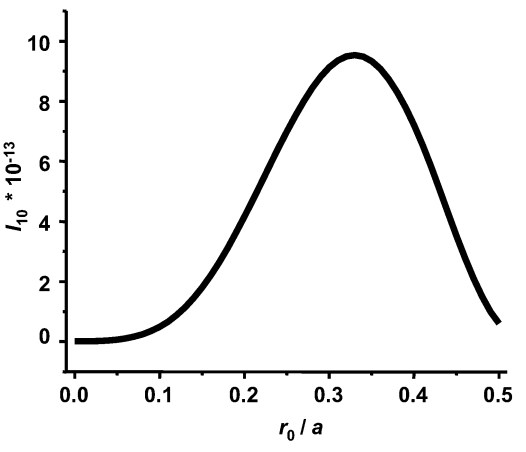

Fig. 3 Intensity of (10) reflection plotted against pore radius normalized to unit cell constant ($\lambda = 0.01$, $a = 10$ nm).

strongly deviating unit cell size the results can differ and relative intensities have to be recalculated.

The influence of the wall thickness for a given unit cell size on the relative intensity of higher indexed reflections normalized to the (10) reflection was calculated. The results are given in Fig. 4. It can clearly be seen that marked differences in relative intensities are expected, depending on the ratio of wall thickness to pore diameter. This can be used to evaluate the wall thickness of ordered mesoporous materials by comparing the experimental patterns with calculated intensity distributions. For MCM-41 synthesized by the Mobil route, typically ratios for (10)/(11) of about 0.06, for (10)/(20) of 0.04–0.05, and for (10)/(21) of below 0.01 are observed. From Fig. 4, indicated by the vertical line, one can then extract the ratio of pore size to wall thickness lying at about 0.38/0.12. Thus, material with a 4 nm pore size would have a wall thickness of around 1.25 nm, which corresponds well to published values. For the acid variant of MCM-41, which is now called SBA-3, typically lower pore sizes are calculated from sorption experiments for the same lattice parameter.[25] These materials often have only very low intensity (11) and (20) reflections, sometimes only the (11) reflection is present and no (20) reflection is visible.[26] Looking at Fig. 4, this corresponds to pore sizes (as fractions of the lattice parameters) around 0.28, which means that the walls for the SBA-3 are thicker than those of MCM-41, which is in line with published data, even considering the shortcomings of pore size analysis in the lower mesopore range (HK pore size 2.8 nm, wall thickness from XRD 1.3 nm;[27] 2.4 nm (presumably BJH) pore size, 1.6 nm wall thickness[28]) and our own work,[29] where the step in the isotherm is below $p/p_0 = 0.2$ (allowing no precise pore size analysis, but presumably around 2 nm) for a lattice parameter of 3.4 nm.

However, the relative intensities depend not only on the ratio between wall thickness and channel diameter and on the unit cell size (see above), but also on the roughness of the pore walls. Fig. 5 shows, how the relative intensities of the higher indexed reflections decrease with increasing smoothing factor λ. The rougher the walls, the lower the relative intensities of the reflections. However, for standard MCM-41 it is not expected that the roughness will be higher than corresponding to a λ exceeding 0.01, since this would correspond to a transition region with a size of about 20% of the wall thickness, and there are no indications for this in the literature (see also Fig. 1). The influence of the wall roughness on the diffraction pattern is thus expected to be comparatively low. This might be different, however, for SBA-15, where the template used and experimental data[22,30] suggest that microporosity is present in the walls, may be near the wall surface. In that case, the roughness would need to be taken into account.

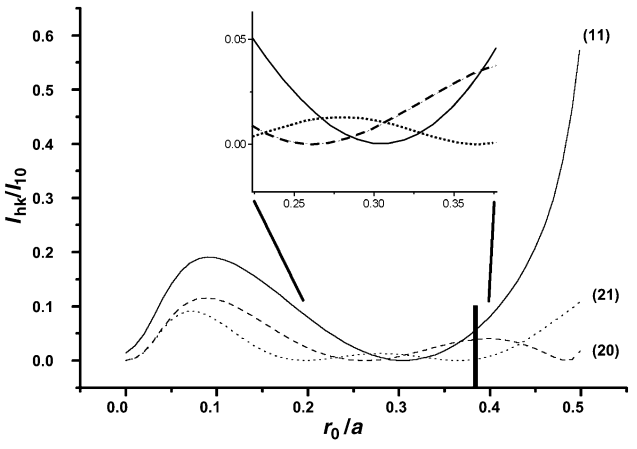

Fig. 4 Relative intensity of higher indexed reflections over normalized pore radius ($\lambda = 0.01$, $a = 10$ nm). The vertical line at $r_0/a = 0.38$ corresponds to regular MCM-41, see text.

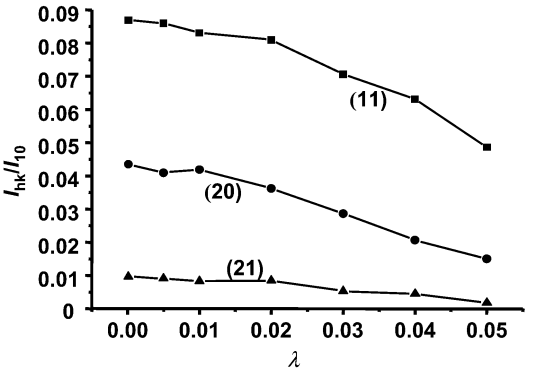

Fig. 5 Relative intensity of higher indexed reflections over smoothing factor λ (eqn. (1)). $r_0 = 4$ nm, $a = 10$ nm.

Composite materials

Template removal from mesostructures. Kleitz *et al.* investigated the behavior of Si-, Ti- and Zr-MCM-41 materials during the calcination process.[31] An increase in intensity of all reflections with increasing temperature was observed for all samples. This can be explained by an increased scattering contrast between the pore walls and the inside of the pores, caused by the burning out of the template. This behavior has been described before and could also be explained by the other X-ray models discussed in the Introduction. During cooling of the transition metal oxide-based materials, however, a loss of scattering intensity is again observed, indicating a loss of scattering contrast. This effect is strongest for the titanium-based material with the smallest pore size, corresponding to a decrease in the (10) reflection intensity by about 35%. This loss is reversible, *i.e.* heating the sample again leads to a recovery of the intensity. With thermogravimetry/mass spectrometry (TG/MS) it could be shown that this is probably due to physisorbed water. The pores of the titania- and zirconia-based materials are much narrower than those of the corresponding silica samples, and the hydrophilicity is higher, so that even pore condensation of water can take place.

The results of the simulations are shown in Fig. 6, where the reflection intensity of the (10) reflection is plotted against the fraction of homogeneously distributed water inside the pores. For these simulations the space in the pores was filled with water molecules with fractional occupancies corresponding to the loading. A water content of around 12% in the calcined sample, as observed experimentally,[31] would thus correspond to a decrease in (10) intensity of around 30%, in good

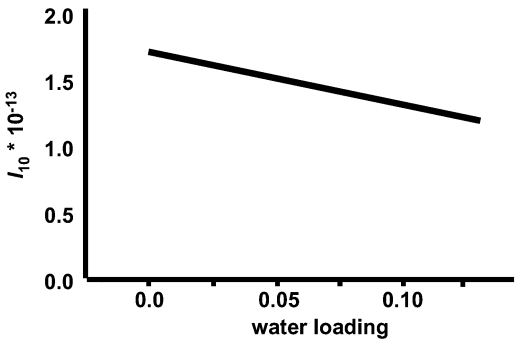

Fig. 6 Intensity of (10) reflection of titanium oxophosphate *versus* water content ($m_{H_2O}/(m_{TiO_2} + m_{H_2O})$). $r_0 = 1$ nm, $a = 3.9$ nm, $\lambda = 0.005$.

agreement with the experimentally observed 35%. As has been shown by the group of Gies, even complete disappearance of the XRD reflections can be induced by filling the pores with highly scattering adsorptives, such as halogenated hydrocarbons.[32]

Coating of SBA-15 with rare-earth oxides. As stated in the Introduction, the motivation to develop the program for the simulation of the diffraction patterns of ordered mesoporous materials was our work on loading SBA-15 and other mesoporous silicas with transition metal or rare earth metal oxides.[7] In our group SBA-15 samples with rare earth metal oxide loadings up to 90 wt.% were investigated. Different analytical techniques indicated a coating of the host material rather than the formation of isolated particles.[8]

At first sight surprisingly, the recorded diffraction patterns of differently loaded materials did not show a continuous change in reflection intensities with increasing rare earth metal oxide content, but rather unexpected variations of the relative intensities of the different reflections. The unmodified material exhibits the (11) and the (20) reflection at low intensity in addition to the high intensity (10) reflection. After a moderate loading, these higher indexed reflections disappear almost completely, and only the (10) reflection is retained. Increasing the loading further, however, leads to a reappearance of the (11) reflection, and, surprisingly, to the appearance of the (21) reflection which could not be distinguished from the background even for the parent material (Fig. 7).

For the simulation a coating of the materials walls with yttria was modeled. The loading to achieve monolayer coverage with yttria can only be estimated, since it requires knowledge of the structure of yttria in the monolayer. Depending on the model used for calculating monolayer coverage, values between 25% and 45% are calculated for the material investigated experimentally.[8] For the simulations

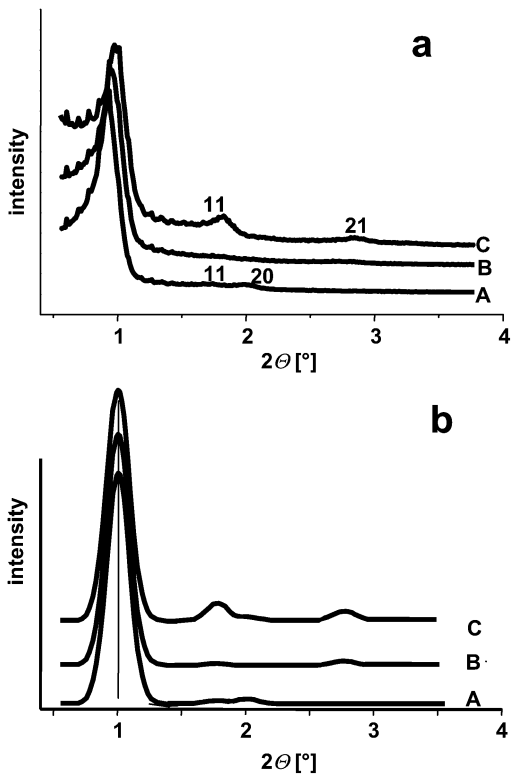

Fig. 7 (a) Experimental XRDs for SBA-15 loaded with increasing amounts of yttria. (A) pure SBA-15, (B) 37% yttria, (C) 59% yttria. (b) Simulated patterns for (A) pure SBA-15, (B) 22% yttria, (C) 35% yttria.

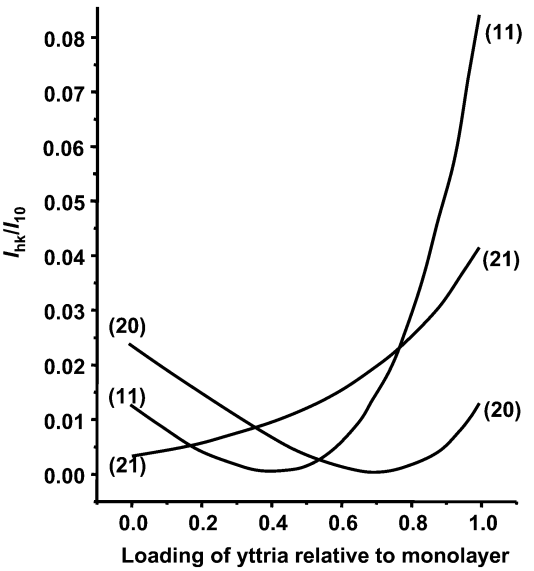

Fig. 8 Relative intensity of higher order reflections *versus* loading with yttria relative to monolayer coverage assumed to be reached at 35%. $r_0 = 3.4$ nm, $a = 10$ nm, yttria layer thickness = 0.6 nm, $\lambda = 0.005$ for all transitions.

here, formation of a monolayer was assumed to be complete at 35%. Loading levels below monolayer coverage were simulated by fractional site occupation factors corresponding to the fraction of the monolayer achieved at a certain loading. Also for the yttria coating a smooth transition was modeled by using Fermi functions on both sides of the layer with $\lambda = 0.005$.

Calculated relative reflection intensities are plotted in Fig. 8 against the loading of SBA-15 with yttria, where a loading of 1 corresponds to the monolayer. The calculation was done for a pore size of 6.0 nm and a wall thickness of 3.2, the experimentally determined values. There is obviously a marked dependence of the different reflection intensities on the yttria coverage. Most characteristic is the initial strong decrease in the (11) and the (20) intensities with increasing yttria loading, corresponding to the disappearance of higher order reflections in the experimental patterns. With higher loading, the (11) intensity recovers, and, also very pronounced, the (21) reflection reaches an intensity which allows it to be distinguished from the background, also in agreement with the experimental data at high loading. The simulations predict the changes in the diffraction pattern at somewhat lower loading levels than experimentally observed. This can be attributed to the uncertainty in the loading necessary to achieve monolayer coverage and the fact that part of the yttria is already present as particles at loadings approaching the monolayer, as seen in the transmission electron micrograph (TEM). Except for this deviation, the correspondence between experimental and simulated patterns, however, is quite satisfactory. The agreement between simulation and experimental results is demonstrated in Fig. 7b, where the simulated patterns corresponding to the experimental data (but at somewhat high loading, see above) in Fig. 7a are given. In order to facilitate comparison, the intensity value of the reflections provided by the program was converted to a Gauss curve to fit the experimental line width. In comparison, simulations in which the site occupation factors in the whole channel were assigned non-zero values, to model a homogeneous yttria distribution as particles in the pores, gave totally unsatisfactory agreement with the experimental data. For this model, a continuous decrease in all reflections with increasing loading was calculated.

These results clearly demonstrate that the model can be used to simulate different types of ordered mesoporous materials

and that the results can be used to help in the interpretation of experimental data.

Conclusions

We have described a simple and flexible method to simulate diffraction patterns of hexagonally ordered mesoporous materials by assuming fully amorphous wall structures. The method allows the simulation of systems with various pore geometries, smooth transitions between wall and pore, and modeling of mesoporous materials loaded with guest species in many configurations. Using this method, different questions concerning the X-ray diffraction properties of ordered mesoporous materials have been addressed and have been satisfactorily answered. In particular, the simulation supports the model of a monolayer coating of SBA-15 with yttria rather than that of separate particles filling part of the void space.

In principle, a similar technique could be used to model the diffraction behavior of the various 3-D ordered mesoporous materials. This will lead to a more complex program but should not pose additional conceptional problems.

References

1 C. T. Kresge, M. E. Leonowicz, W. J. Roth, J. C. Vartuli and J. S. Beck, *Nature*, 1992, **359**, 710.
2 T. Yanagisawa, T. Shimizu, K. Kuroda and C. Kato, *Bull. Chem. Soc. Jpn.*, 1990, **63**, 988.
3 F. Schüth, *Stud. Surf. Sci. Catal.*, 2001, **35**, 1.
4 G. Oye, J. Sjoblom and M. Stöcker, *Adv. Colloid Interface Sci.*, 2001, **89**, 439.
5 U. Ciesla and F. Schüth, *Microporous Mesoporous Mater.*, 1999, **27**, 131.
6 J. Y. Ying, C. P. Mehnert and M. S. Wong, *Angew. Chem. Int. Ed. Engl.*, 1999, **38**, 56.
7 F. Schüth, A. Wingen and J. Sauer, *Microporous Mesoporous Mater.*, 2001, **44–45**, 465.
8 J. Sauer, F. Marlow, B. Spliethoff and F. Schüth, *Chem. Mater.*, in press.
9 J. S. Beck, J. C. Vartuli, W. J. Roth, M. E. Leonowicz, C. T. Kresge, K. D. Schmitt, D. T.-W. Chu, D. H. Olson, E. W. Sheppard, S. B. McCullen, J. B. Higgins and J. L. Schlenker, *J. Am. Chem. Soc.*, 1992, **114**, 10 834.
10 G. Oster and D. P. Riley, *Acta. Crystallogr.*, 1952, **5**, 272.
11 J. V. Smith and D. J. Dytrych, *Nature*, 1984, **209**, 607.
12 G. Stucky, A. Monnier, F. Schüth, Q. Huo, D. Kumar, D. Margolese, M. Krishnamurty, P. Petroff, A. Firouzi, M. Jaenicke and B. Chmelka, *Mol. Cryst. Liq. Cryst.*, 1994, **240**, 187.
13 V. Alfredsson, M. Keung, A. Monnier, G. Stucky, K. Unger and F. Schüth, *J. Chem. Soc., Chem. Commun.*, 1994, 921.
14 L. A. Solovyov, S. D. Kirik, A. N. Shmakov and V. N. Romannikov, *Microporous Mesoporous Mater.*, 2001, **44–45**, 17.
15 B. P. Feuston and J. B. Higgins, *J. Phys. Chem.*, 1994, **98**, 4459.
16 K. Kleestorfer, H. Vinek and A. Jentys, *J. Mol. Catal. A*, 2001, **166**, 53.
17 C. Pophal and H. Fuess, *Microporous Mesoporous Mater.*, 1999, **33**, 241.
18 S. Schacht, M. Janicke and F. Schüth, *Microporous Mater.*, 1998, **22**, 485.
19 W. Hammond, E. Prouzet, S. D. Mahanti and T. J. Pinnavaia, *Microporous Mesoporous Mater.*, 1999, **27**, 19.
20 Z. Tun and P. C. Mason, *Acta. Crystallogr. Sect. A*, 2000, **56**, 536.
21 K. J. Edler, P. A. Reynolds, J. W. White and D. Cookson, *J. Chem. Soc., Faraday Trans.*, 1997, **93**, 199.
22 M. Imperor-Clerc, P. Davidson and A. Davidson, *J. Am. Chem. Soc.*, 2000, **122**, 11 925.
23 *International Tables of X-ray Crystallography*, ed. T. Hahn, Kluwer, Dordrecht, 1996, vol. A.
24 H. P. Klug and L. E. Alexander, *X-ray Diffraction Procedures*, Wiley, New York, 2nd edn., 1974.
25 Q. Huo, D. I. Margolese, U. Ciesla, P. Feng, T. E. Gier, P. Sieger, R. Leon, P. M. Petroff, F. Schüth and G. D. Stucky, *Nature*, 1994, **368**, 317.
26 T. R. Pauli, Y. Liu, T. J. Pinnavaia, S. J. L. Billinge and T. P. Rieker, *J. Am. Chem. Soc.*, 1999, **121**, 8835.
27 S. S. Kim, Y. Liu and T. J. Pinnavaia, *Microporous Mesoporous Mater.*, 2001, **44–45**, 489.
28 L. R. Dai, T. W. Wang, L. T. Bu and G. Chen, *Colloids Surf. A*, 2001, **181**, 151.
29 S. Disser, U. Junges, S. Schacht, W. Schmidt, F. Schüth, M. Thieme and A. Wingen, unpublished results.
30 C. G. Göltner, B. Smarsley, B. Berton and M. Antonietti, *Chem. Mater.*, 2001, **13**, 1617.
31 F. Kleitz, W. Schmidt and F. Schüth, *Microporous Mesoporous Mater.*, 2001, **44–45**, 95.
32 B. Marler, U. Oberhagemann, S. Vortmann and H. Gies, *Microporous Mater.*, 1996, **6**, 375.